Blucher Mechanical Engineering Proceedings
May 2014, vol. 1 , num. 1
www.proceedings.blucher.com.br/evento/10wccm

10th World Congress on Computational Mechanics
8-13 July 2012 • São Paulo • Brazil

PARALLEL COMPUTATION FOR FLUID-STRUCTURE THERMAL INTERACTIONS WITH MULTIPHASE MODELING

K. Maruyama[1], D. Toriu[1] and S. Ushijima[2]

[1] Civil and Earth Resources Eng., Kyoto University, Japan
[2] ACCMS, Kyoto University, Japan

Abstract. *This paper presents a computational method to predict gas-liquid-solid multiphase phenomena. In addition to the mechanical interactions between the different phases, their thermal interactions are taken into account in the present multiphase modeling. The phase-averaged governing equations, including the energy equation to predict temperature distributions, are discretized with a finite volume method and calculated with the numerically stable and accurate algorithms. The numerical procedures are parallelized with flat MPI so that it can be executed on recent large-scale distributed memory systems. It was applied to basic engineering problems and its validity was discussed.*

Keywords: *thermal interaction, multiphase modeling, parallel computation*

1. INTRODUCTION

It is essential to predict accurately the interactions between gas-liquid flows and solid objects in many engineering subjects. In this paper, a computational method is investigated to predict gas-liquid-solid multiphase phenomena, in which thermal interactions become important in addition to the mechanical effects among the phases.

The governing equations for a multiphase field, in which each phase is incompressible and immiscible, are derived taking account of the energy equations among different phases like a one-fluid model [1]. Since the derived multiphase model is applicable to the free-surface flows including complicated-shaped solid objects with structured grid system, the numerical procedure becomes robust and simple. The governing equations are discretized with a finite volume method and the numerical solutions are obtained with an SMAC method. In particular, a collocated grid system is utilized so that the parallel computational method can be easily implemented on the basis of the 3D domain decomposition method using flat MPI.

The computational method was applied to the natural convection around a rectangular fin and the predicted fin efficiency was compared with the theoretical values. In addition, numerical experiment was conducted for the non-isothermal gas-liquid-solid multiphase field, in which gas and liquid flows are caused by the initial temperature difference in the computational area including a vertical cylinder with heat conduction. As a result, it was demonstrated that the present method is applicable to the multiphase field including thermal interactions.

2. NUMERICAL PROCEDURES

2.1. Governing equations

As shown in Fig.1, we consider the multiphase field consisting of gas, liquid and solid phases, where each phase is incompressible and they are immiscible. In Fig.1, Ω and Ω_k stand for the volumes in the whole area and the phase-k, respectively, where Ω is equal to $\sum_k \Omega_k$.

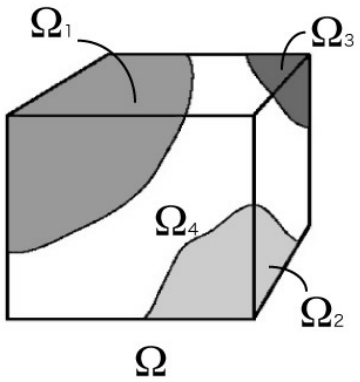

Figure 1. Multiphase field including different phases

Assuming that the internal energy U is given by $C_v T$, where C_v and T are specific heat under constant volume and temperature, the governing equation for T can be derived from the law of energy conservation using Fourier's law of heat conduction. It is assumed that there are no heat sources or sinks. Taking account of the incompressibility and neglecting the change of energy due to fluid viscosity, a set of averaged governing equations for the non-isothermal multiphase field can be obtained in the similar way to one-fluid model. They consist of mass conservation equation in Eulerian description, incompressible condition, momentum equation and energy equation given by

$$\frac{\partial \rho}{\partial t} + \frac{\partial (\rho u_i)}{\partial x_i} = 0 \tag{1}$$

$$\frac{\partial u_i}{\partial x_i} = 0 \tag{2}$$

$$\frac{\partial u_i}{\partial t} + \frac{\partial (u_i u_j)}{\partial x_j} = -\frac{1}{\rho}\frac{\partial p}{\partial x_i} + g_i + \frac{1}{\rho}\frac{\partial}{\partial x_j}\left[\frac{\partial (\mu u_i)}{\partial x_j} + \frac{\partial (\mu u_j)}{\partial x_i}\right] \tag{3}$$

$$\frac{\partial T}{\partial t} + \frac{\partial (T u_i)}{\partial x_i} = \frac{\partial}{\partial x_i}\left(\alpha \frac{\partial T}{\partial x_i}\right) \tag{4}$$

where t is time, x_i is the i-th component of three-dimensional orthogonal coordinates and g_i is the acceleration of external force in x_i direction. While the velocity component u_i is

the mass-averaged value in the mixture of fluids, volume-averaged variables are defined for density ρ, pressure p, viscosity μ, temperature T and thermal diffusivity α. For example, u_i and α are defined as

$$u_i = \frac{\sum_k \rho_k \Omega_k u_{i,k}}{\sum_k \rho_k \Omega_k} \quad \text{and} \quad \alpha = \frac{\sum_k \Omega_k \alpha_k}{\Omega} \tag{5}$$

In the actual computation, Ω_k is estimated with the sub-cell method [2].

The density in the above equations is a function of temperature $\rho = \rho(T)$. In case that the density differences are sufficiently small, on the other hand, the Boussinesq approximation is applicable to Eq.(3); ρ and g_i in Eq.(3) are expressed as ρ_0 and $g_i\beta(T - T_0)$ respectively, where subscript $''0''$ means reference constant values and β is the volume coefficient of expansion.

2.2. Computational method

The numerical procedures of the incompressible fluid-mixture consist of three steps: prediction, pressure-computation and correction stages. In the prediction stage, the tentative velocity component u_i^* is calculated at the center of the fluid-cells with a finite-volume method. In this procedure, Eq.(3) is discretized with the C-ISMAC method [3], which is based on the implicit SMAC method [4]. The equation discretized with respect to time by the C-ISMAC method is given by

$$\begin{aligned}\frac{u_i^* - u_i^n}{\Delta t} &= g_i - \frac{1}{\rho}\frac{\partial p^n}{\partial x_i} - \gamma_1 \frac{\partial}{\partial x_j}(u_i^* u_j^n) - (1-\gamma_1)\frac{\partial}{\partial x_j}(u_i^n u_j^n) \\ &+ \frac{\gamma_2}{\rho}\frac{\partial}{\partial x_j}\left[\frac{\partial}{\partial x_j}(\mu u_i^*) + \frac{\partial}{\partial x_i}(\mu u_j^*)\right] + \frac{1-\gamma_2}{\rho}\frac{\partial}{\partial x_j}\left[\frac{\partial}{\partial x_j}(\mu u_i^n) + \frac{\partial}{\partial x_i}(\mu u_j^n)\right]\end{aligned} \tag{6}$$

where γ_1 and γ_2 are parameters whose ranges are $0 \le \gamma_1, \gamma_2 \le 1$. The tentative velocity component u_i^* can be written as the following relationship:

$$u_i^* = u_i^n + \tilde{u}_i \tag{7}$$

With Eq.(7), we can transform Eq.(6) to the following equation:

$$\begin{aligned}&\frac{\tilde{u}_i}{\Delta t} + \gamma_1 \frac{\partial}{\partial x_j}(\tilde{u}_i u_j^n) - \frac{\gamma_2}{\rho}\frac{\partial}{\partial x_j}\left[\frac{\partial}{\partial x_j}(\mu \tilde{u}_i) + \frac{\partial}{\partial x_i}(\mu \tilde{u}_j)\right] \\ &= g_i - \frac{1}{\rho}\frac{\partial p^n}{\partial x_i} - \frac{\partial}{\partial x_j}(u_i^n u_j^n) + \frac{1}{\rho}\frac{\partial}{\partial x_j}\left[\frac{\partial}{\partial x_j}(\mu u_i^n) + \frac{\partial}{\partial x_i}(\mu u_j^n)\right]\end{aligned} \tag{8}$$

where $\tilde{u}_i$ becomes nearly zero when the flow field is almost steady or the time-scale of the flow field is sufficiently larger than the time increment Δt. Thus, we can apply a simple first-order spatial discretization method to the left-hand side of Eq.(8), while a higher-order scheme to the right-hand side. The convection terms are evaluated with a fifth-order TVD scheme [5]. The C-ISMAC method enables us to derive easily the simultaneous equation system from the implicit form of the left-hand side of Eq.(8) as well as to preserve numerical accuracy by applying a higher-order scheme to the explicit form on the right-hand side of the same equation.

After solving the equation system of $\tilde{u}_i$, which is derived from the discretized equation of Eq.(8), u_i^* is determined with Eq.(7). The u_i^* located at the center of the fluid-cell is then spatially interpolated on the cell boundary. Before this interpolation, pressure-gradient term evaluated at the cell center is removed from u_i^* in order to prevent pressure oscillation as

$$\hat{u}_i = u_i^* + \frac{1}{\rho}\frac{\partial p^n}{\partial x_i}\Delta t \tag{9}$$

The cell-center velocity $\hat{u}_i$, which is evaluated without the pressure-gradient term, is spatially interpolated on the cell boundaries by a suitable function f_b. After this procedure, the pressure-gradient terms, which are estimated on the cell boundaries, are added to the interpolated velocity, $f_b(\hat{u}_i)$. Thus, we obtain the cell-boundary velocity component $u_{b,i}$ as follows:

$$u_{b,i} = f_b(\hat{u}_i) - \left.\frac{1}{\rho}\frac{\partial p^n}{\partial x_i}\right|_b \Delta t \tag{10}$$

The velocity component $u_{b,i}^{n+1}$ at $n+1$ time-step is defined by

$$u_{b,i}^{n+1} = f_b(\hat{u}_i) - \left.\frac{1}{\rho}\frac{\partial p^{n+1}}{\partial x_i}\right|_b \Delta t \tag{11}$$

Subtracting Eq.(18) from Eq.(11), we have

$$u_{b,i}^{n+1} = u_{b,i} - \frac{1}{\rho}\frac{\partial \phi}{\partial x_i}\Delta t \tag{12}$$

where $\phi = p^{n+1} - p^n$. Substitution of Eq.(12) into Eq.(2) yields the following equation of ϕ :

$$\frac{\partial}{\partial x_i}\left(\frac{1}{\rho}\frac{\partial \phi^k}{\partial x_i}\right) = \frac{1}{\Delta t}\frac{\partial u_{b,i}}{\partial x_i} \equiv \frac{D}{\Delta t} \tag{13}$$

At the pressure-computation stage, Eq.(13) is solved with the C-HSMAC method [1]. The relationships in the C-HSMAC method are given by

$$\frac{\partial}{\partial x_i}\left(\frac{1}{\rho}\frac{\partial \phi}{\partial x_i}\right) = \frac{D^k}{\Delta t} \tag{14}$$

$$p^{k+1} = p^k + \phi \tag{15}$$

$$u_{b,i}^{k+1} = u_{b,i}^k - \frac{\Delta t}{\rho}\frac{\partial \phi}{\partial x_i} \tag{16}$$

where the superscript k stands for the iteration step-number of the C-HSMAC method. The C-HSMAC method enables us to obtain the pressure and cell-boundary velocity components, which satisfy the incompressible condition $|D| < \epsilon_D$ in each computational cell, where ϵ_D is a given threshold. While the final results of the C-HSMAC method are similar to those of the SOLA method [6], it has been proved that the computational efficiency of the C-HSMAC method is largely improved [7].

The discretization of Eq.(14) yields simultaneous linear equation system of ϕ, which is solved with the BiCGSTAB method [8]. The iterative computation using the above three equations is continued until $|D| < \epsilon_D$ is satisfied in all fluid-cells.

A parallel computational method is employed on the basis of the 3D domain decomposition method. All procedures shown above are parallelized with flat MPI (Message-Passing Interface) [9] in order to utilize the recent large-scale distributed-memory system. Since the convection terms included in the governing equations are solved with a higher-order scheme, the overlapping cells having necessary width are placed around each sub-domain. The message passings are conducted mainly in the implicit computations for the C-ISMAC method and pressure computations with the C-HSMAC method.

3. APPLICATION OF PREDICTION METHOD

The above computational method was applied to two phenomena. The first one is the natural convection around a straight fin of rectangular profile on a plane wall with 2D model using Boussinesq approximation. The second example is the 3D thermal and mechanical interactions among gas, liquid and solid phases, which was predicted by parallel computations without Boussinesq approximation.

3.1. Natural convection around a rectangular fin

Figs. 2 and 3 show the computational area and a rectangular fin. The lengths l_1 and l_2 are 40 mm, the half thickness y_b of the fin is 1 mm and the initial temperature T_0 of the liquid around the fin is fixed at 273 K, while the base temperature T_1 and the length of the fin W vary among T_1 = 283, 373, 773 K and W = 6, 16, 32 mm independently. The materials of fin and surrounding fluid are assumed to be aluminum and water. Their approximate physical properties actually used in the calculations are listed in Tables 1 and 2. On the wall boundary, adiabatic and non-slip conditions are imposed. The numbers of fluid cells are 100 $\times$ 100.

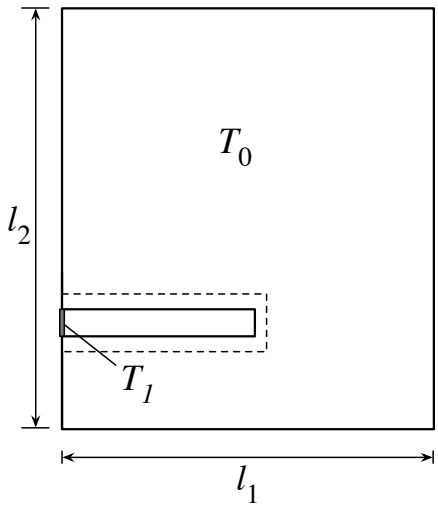

Figure 2. 2D computational area

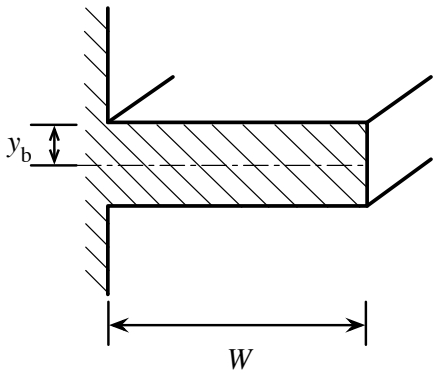

Figure 3. Rectangular fin

Table 1. Physical properties of fin

density (kg/m^3)	thermal diffusivity (m^2/s)
2.69×10^3	9.77×10^{-5}

Table 2. Physical properties of surrounding fluid

density (kg/m^3)	viscosity (Pa·s)	thermal diffusivity (m^2/s)	volume coefficient of expansion ($1/K$)
0.998×10^3	1.03×10^{-3}	1.44×10^{-5}	2.07×10^{-4}

Fig.4 shows the predicted results in case that W = 15 mm. Only the base temperature of the fin is kept at T_1 = 373 K in Fig.4 (a), whereas the entire temperature of the fin is fixed at T_1 = 373 K in Fig.4 (b). The calculations are performed until the heat per unit time Q, transferred between the fin and the fluid, becomes nearly constant. As shown in Fig.4, it can be seen that the heat conduction in the fin and surrounding natural convection are reasonably predicted with the present method.

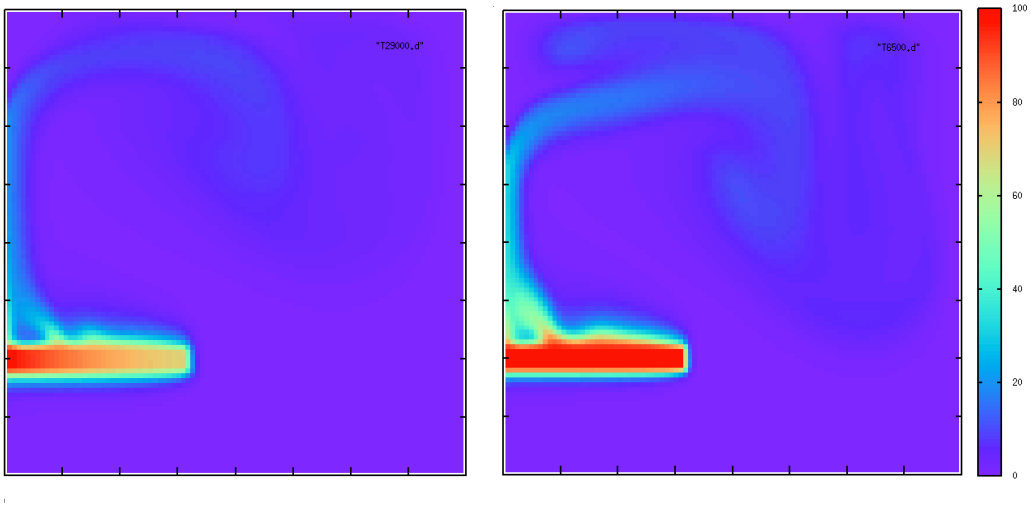

(a) Heat-conduction fin (b) Isothermal fin

Figure 4. Temperature distribution in fin and surrounding fluid
(number of color bar = $T - T_0$)

The predicted results are quantitatively compared with the theoretical solution in terms of the fin efficiency η [10] defined by

$$\eta = \frac{Q_1}{Q_2} \tag{17}$$

where Q_1 is the actually transferred heat per time, whereas Q_2 is the one which would be transferred if entire fin area were at base temperature. Thus, η corresponds to the ratio of the heat per time shown in Fig.4 (a) to that shown in Fig.4 (b). The fin efficiency depends on u_b which is determined by the shape and physical properties of the fin as follows:

$$u_b = W\sqrt{\frac{h_m}{\lambda y_b}} \tag{18}$$

with

$$h_m = \frac{Q_2}{A(T_1 - T_0)} \tag{19}$$

where h_m corresponds to the heat transfer coefficient averaged over the perimeter A of the fin. The theoretical relationship between u_b and η is given by the following equation [10]:

$$\eta = \frac{\tanh u_b}{u_b} \tag{20}$$

The above equation is derived assuming that the end of the fin is insulated so that $\partial T/\partial x = 0$.

Fig.5 shows the comparison between the predicted results and Eq.(20). As shown in Fig.5, the predicted results are almost in good agreement with theoretical solutions.

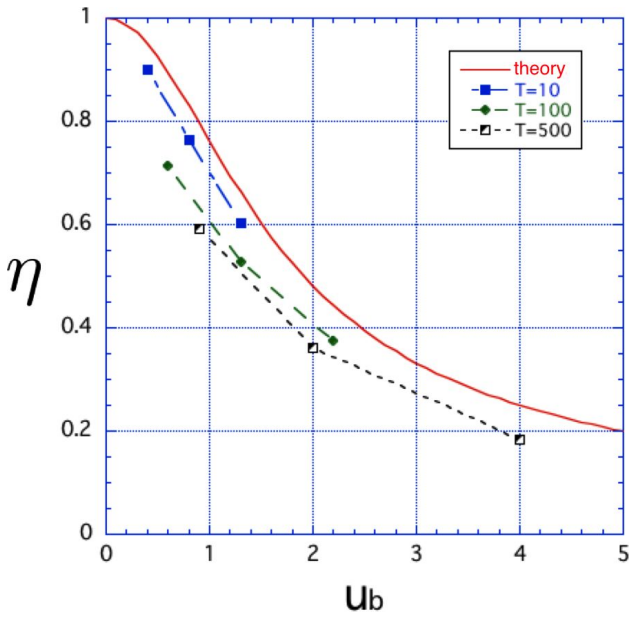

Figure 5. Relationship between fin efficiency η and u_b
(Three predicted results in each group are ranged W = 6, 16 and 32 (mm) from left to right. T in the legend = $T_1 - T_0$.)

3.2. Thermal interaction in 3D multiphase field

The computational method was applied to the gas-liquid-solid multiphase field having temperature distributions. As shown in Fig.6 (a), the cubic computational area ($l_1 = l_2 =$

$l_3 = 3.0$ m and $h_1 = h_2 = 1.5$ m) consists of gas and liquid phases including a vertical cylinder with $d = 1.0$ m. Since the shape of a solid object is represented with multiple tetrahedron elements to deal with complicated-shaped objects, the cylinder is treated with such elements in this calculation as well.

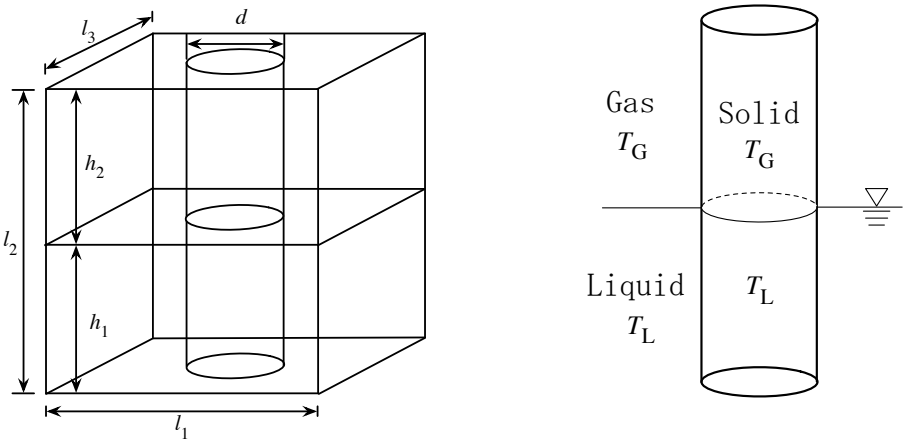

(a) 3D computational area (b) Initial temperature distribution

Figure 6. 3D computational area and initial temperature distributions

In the initial condition, the gas and liquid phases are in a static state. Hereafter, the subscripts G, L and S stand for the variables of gas, liquid and solid phases respectively. In the present calculations, the Boussinesq approximation is not used and the density ρ in Eq.(3) is represented as a linear function of temperature with a constant volume coefficient of expansion β as

$$\rho = \rho_0 \left[1 + \beta(T - T_0)\right] \tag{21}$$

where $T_0 = 273$ (K), ρ_{0G} and ρ_{0L} are 1.0 and 10^3 (kg/m^3), β_G and β_L are 1.0×10^{-3} and 1.0×10^{-4} (1/K). In addition, the thermal diffusivities α_G, α_L and α_S are 1.0×10^{-5}, 1.0×10^{-7} and 1.0×10^{-4} (m^2/s) respectively.

The initial temperatures of gas and liquid phases are set as $T_G = 273.0$ (K) and $T_L = 283.0$ (K). In the cylinder, the vertical distribution of the initial temperature is same as those of the gas and liquid phases as shown in Fig.6 (b). Since the initial conditions for gas and liquid phases are unstable in terms of the temperature distribution, the buoyancy-driven downward flow arises in the liquid phase when it is cooled on the free surface by the lower-temperature gas. Due to the large thermal diffusivity in the cylinder, its initial temperature distribution is diffused rapidly in the vertical direction.

The parallel computation is conducted with 3D domain decomposition. The predicted results are shown in Figs.7 and 8. The temperature of the liquid phase near the free surface decreases due to the cold gas. The cooled liquid moves downward to the bottom surface. This flow pattern is observed away from the high-thermal-diffusivity cylinder. One of the factors that cause this flow pattern is the fact that the temperature difference between gas and liquid phases is decreased by the thermal interaction with the cylinder in the horizontal direction.

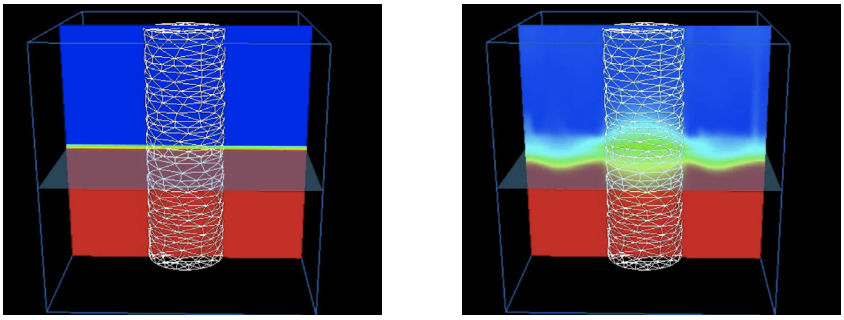

(a) $t = 0.0$ (s) (b) $t = 10.0$ (s)

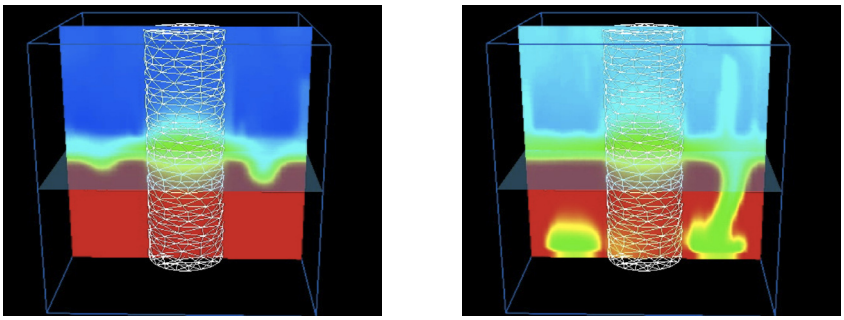

(c) $t = 15.0$ (s) (d) $t = 30.0$ (s)

Figure 7. Predicted temperature distributions on vertical sections

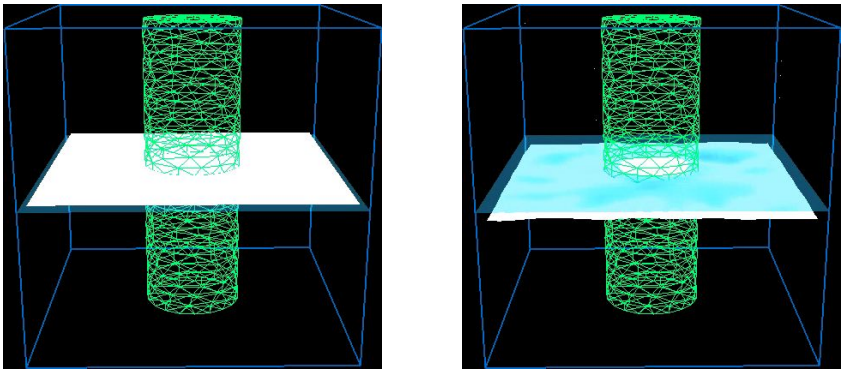

(a) $t = 0.0$ (s) (b) $t = 10.0$ (s)

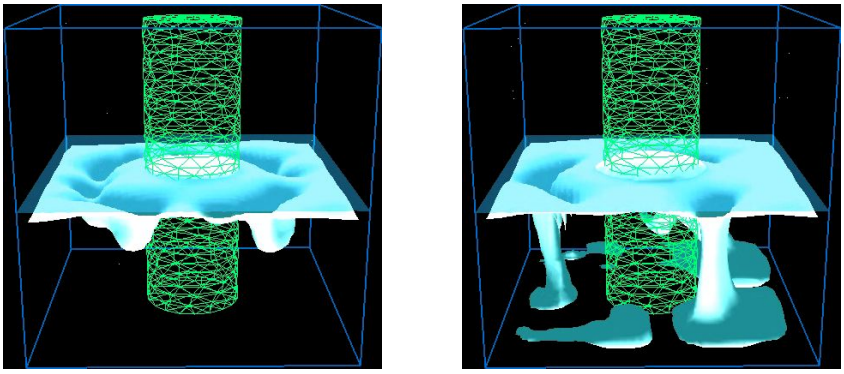

(c) $t = 15.0$ (s) (d) $t = 30.0$ (s)

Figure 8. Predicted isothermal surfaces (Temperature of surface = 278 K)

4. CONCLUSIONS

In this paper, a computational method was investigated to predict gas-liquid-solid multiphase phenomena taking account of their thermal interactions. The phase-averaged governing equations, including the energy equation, are discretized with a finite volume method and solved with the SMAC algorithm in which some new techniques have been implemented. To deal with large-scale problems, the computational method was parallelized with the flat MPI.

The computational method was applied to the natural convection around a rectangular fin and the predicted fin efficiency was compared with the theoretical values. In addition, numerical experiment was conducted for the gas-liquid flows having different initial temperatures in the computational area including a vertical cylinder with heat conduction. As a result, it is demonstrated that the present method is applicable to the multiphase field including thermal interactions.

References

[1] S. Ushijima. Multiphase-model approach to predict arbitrarily-shaped objects moving in free surface flows. *Proc of APCOM'07 – EPMESC XI*, pages MS41–3–1, 2007.

[2] S. Ushijima and N. Kuroda. Multiphase modeling to predict finite deformations of elastic objects in free surface flows. *Fluid Structure Interaction V, WIT Press*, pages 34–45, 2009.

[3] S. Ushijima and I. Nezu. Higher-order implicit (C-ISMAC) method for incompressible flows with collocated grid system. *JSCE Journal*, (719/II-61):21–30, 2002.

[4] B. R. Shin, T. Ikohagi, and H. Daiguji. An unsteady implicit SMAC scheme for two-dimensional incompressible Navier-Stokes equations. *JSME International Journal*, 36(4):598–606, 1993.

[5] S. Yamamoto and H. Daiguji. Higher-order-accurate upwind schemes for solving the compressible Euler and Navier-Stokes equations. *Computers Fluids*, 22(2/3):259–270, 1993.

[6] C. W. Hirt and J. L. Cook. Calculating three-dimensional flows around structures and over rough terrain. *J. Comput. Phys.*, 10:324–340, 1972.

[7] S. Ushijima, S. Yamada, S. Fujioka, and I. Nezu. Prediction method (3D MICS) for transportation of solid bodies in 3D free-surface flows. *JSCE Journal*, 810/II-74:79–89, 2006.

[8] H. A. Van Der Vorst. BI-CGSTAB : A first and smoothly converging variant of BI-CG for the solution of nonsymmetric linear systems. *SIAM J. Sci. Stat. Comput.*, 13:631–644, 1992.

[9] W. Gropp, E. Lusk, and R. Thakur. *Using MPI-2*. The MIT Press, 1999.

[10] J. P. Holman. *Heat Transfer*. McGRAW-HILL, INC., 1997.